INSTITUTE OF PHYSICS PUBLISHING NETWORK: COMPUTATION IN NEURAL SYSTEMS

Network: Comput. Neural Syst. **13** (2002) 343–356 PII: S0954-898X(02)38890-0

Comparison of semi-automatic and automatic data acquisition methods for studying three-dimensional distributions of large neuronal populations and axonal plexuses

Sveinung Lillehaug, Daniel Øyan, Trygve B Leergaard and Jan G Bjaalie[1]

Neural Systems and Graphics Computing Laboratory, Department of Anatomy, Institute of Basic Medical Sciences, University of Oslo, PO Box 1105, Blindern, N-0317 Oslo, Norway

E-mail: j.g.bjaalie@basalmed.uio.no

Received 17 April 2002
Published 30 July 2002
Online at stacks.iop.org/Network/13/343

Abstract

Neuroanatomy is in need of high throughput methods for reliably recording the distribution of tissue elements across large brain regions. We compared two methods for recording the spatial distribution of identified neuronal elements such as tracer labelled cell bodies or axonal plexuses. The methods compared were computerized image-combining microscopy (semi-automatic method), which is a user controlled method providing feedback during digitization, and digital camera technology with image analysis software (automatic method). Both methods were applied to biotinylated dextran amine labelled axonal plexuses and FluoroRuby labelled neuronal cell bodies, in the pontine nuclei of the rat. Coordinates were assigned to the labelled elements using both methods. The ensuing distribution patterns were compared, section by section, and in three-dimensional reconstruction. The experienced investigator, using the semi-automatic method, could detect individual axons, fragments of axons, weakly labelled elements, and overlapping cell bodies, better than the automatic system. Nevertheless, both methods detected the overall distribution of the labelled axons and cells investigated. Automatic methods provide opportunities for efficient large-scale data acquisition of labelled neuronal elements.

1. Introduction

Systems neuroanatomy deals with the organization of brain regions and cell populations. Cells in the nervous system can be divided into numerous groups according to a variety of criteria,

[1] Author to whom any correspondence should be addressed.

such as presence of specific molecules, input and output relationships, or morphological characteristics. Among techniques used to identify structures in the brain are *in situ* hybridization, immunocytochemistry, axonal tracing (tract tracing) and various routine staining methods (see, e.g. Glover *et al* 1986, Heimer and Zaborszky 1989, Danbolt *et al* 1998, Armstrong and Hawkes 2000, Köbbert *et al* 2000, Reiner *et al* 2000, Swanson 2000, Van Haeften and Wouterlood 2000, Zaborszky and Duque 2000). To study the localization of large populations of cells or axonal plexuses distributed across multiple serial sections, spatial coordinates need to be assigned to the labelled structures.

Point representations are useful for studying distributions of large populations of cells (see, e.g., Bjaalie *et al* 1991, He *et al* 1993, Flaherty and Graybiel 1994, Nikundiwe *et al* 1994, Malmierca *et al* 1995, Vassbø *et al* 1999, Brevik *et al* 2001, Nadasdy and Zaborszky 2001), and can also be employed for coding the distribution of labelled axonal plexuses (Leergaard *et al* 1995, 2000a, 2000b, Malmierca *et al* 1998, Alloway *et al* 1998, 2000). Multiple methods are used for allocating spatial coordinates to elements in tissue sections (for a review, see Bjaalie 1992). One of the most commonly used methods is computerized image-combining microscopy (Glaser *et al* 1979, 1983, Glaser and Glaser 1990, Leergaard and Bjaalie 1995). This is a semi-automatic method based on the mixing of the image of the specimen and a computer-generated drawing area. The motorized microscope stage and software employed with this method permits synchronous movement of the specimen image and drawing area, thus providing feedback to the user about the digitization process. This method allows digitization of spatial positions with high resolution and accuracy across large brain regions. The method is, however, time consuming and tedious for larger datasets. This is an important restriction for quantitative analyses and large-scale mapping studies that require accumulation of data from many sections and experiments. Thus, there is a need for high-throughput and reliable data acquisition methods that are less dependent on human pattern recognition capabilities. Automated image analysis techniques have been applied for, e.g. segmentation of cytoarchitectonic boundaries in the cerebral cortex (Wree *et al* 1982, Schleicher and Zilles 1990, Grefkes *et al* 2001, Amunts and Zilles 2001, Rademacher *et al* 2001), and delineation of the boundaries of labelled axonal plexuses (Schwarz and Thier 1995, Schwarz and Möck 2001).

In this paper, we compare the recording precision and speed provided by the image-combining method with that provided by digital camera technology in combination with image analysis software, referred to as an automatic method (for a review, see e.g., Inoué and Spring 1997). We employed a fluorescent tracer to label neuronal cell bodies and a light microscopic tracer to label axonal plexuses. The same tissue sections were analysed with both the semi-automatic and automatic methods and the results directly compared. One of the comparisons included a full 3D reconstruction of the patterns of labelling identified in a large brain stem nucleus. We conclude that the automatic method is suitable for mapping of large number of elements across multiple sections. Advantages and limitations of both methods are discussed.

2. Experimental material

Material from two adult female Sprague Dawley rats were used. All animal procedures were reviewed by the local institutional animal welfare committee and were in compliance with national laws and with National Institutes of Health guidelines for the use and care of laboratory animals. Results from one animal were previously reported in Leergaard *et al* (2000b), animal R118. The 3D coordinate data from this case were downloaded from our data repository, at http://www.nesys.uio.no. Surgical anaesthesia was obtained by intramuscular injection of 0.20–0.25 ml kg^{-1} of a mixture of 25% ketamine hydrochloride (100 mg ml^{-1}), 6.3%

xylazine (20 mg ml^{-1}), and 0.25% acepromazine maleate (10 mg ml^{-1}) in physiological saline, followed by intraperitoneal injection of sodium pentobarbital (50 mg ml^{-1}; 0.05–0.06 ml kg^{-1}). Restricted regions of the cerebral or cerebellar cortex were exposed by craniotomy and incision of the dura, and injected with dextran amine neural tracers (see below). After 1 week survival, the animals were re-anaesthetized and perfused with lukewarm saline followed by 4% paraformaldehyde and 10% sucrose (all solutions were phosphate buffered). The brains were removed, photographed and soaked in 30% sucrose for 1 day prior to sectioning. Transverse sections through the injected cerebral and cerebellar regions respectively, and through the brain stems of the two cases, were cut at 50 μm on a freezing microtome. For the purpose of 3D reconstruction (see below), a complete series of sections through the pontine nuclei were collected. One animal was injected with biotinylated dextran amine (BDA; Molecular Probes, Eugene, OR) in the primary somatosensory cortex. BDA labelling was visualized histochemically according to steps 1–7 in Lanciego and Wouterlood (1994) with modifications explained in Leergaard *et al* (2000b). Anterogradely labelled axonal fibres and anatomic landmarks were observed in the pontine nuclei by conventional light microscopy. The other animal was injected with rhodamine conjugated dextran amine (FluoroRuby, FR; Molecular Probes, Eugene, OR) in the cerebellar cortical region crus IIa. Retrogradely labelled neurons were viewed in several brain stem locations, including the pontine nuclei and the trigeminal nuclei, using a Zeiss Axioskop II microscope providing excitation light of 534–558 nm (Zeiss filter set no 15). Anatomic landmarks were recognized by differences in auto-fluorescence.

3. Basic technology

3.1. Semi-automatic data acquisition: computerized image-combining microscopy

The principle of computerized image-combining microscopy was introduced by Glaser and Van der Loos (Glaser *et al* 1979, 1983) and has been implemented by several investigators and companies (Capowski 1985, 1989, Glaser and Glaser 1990, Leergaard and Bjaalie 1995). In the context of the present investigation, the essential components of the graphical user interface are the screen cursor, the drawing area, and the multiple icons used to categorise the different objects to be recorded (e.g., dotted symbols and lines used to code the different categories of labelled cells, surfaces and boundaries, in the specimen). The monitor, displaying the user interface, is projected into the microscope field of view via the drawing tube. Alternatively, with the use of a camera, the image of the specimen is mixed with that of the drawing area. Digitization is performed by pointing the mouse-controlled cursor at each point of interest. Graphical symbols are superimposed on the digitized objects. Thus, the user views the specimen with an overlay of lines and dots. As the stage position is changed, the superimposed graphical symbols move synchronously with the image of the specimen. To maintain correct position of the graphical overlay in relation to the specimen, the magnification of the graphical image is accurately calibrated to match the magnification of the specimen in the microscope field of view. An example of a system configuration is detailed in Leergaard and Bjaalie (1995).

The software for image-combining microscopy used in the present study was MicroTrace (Leergaard and Bjaalie 1995) and Neurolucida (MicroBrightField, Colchester, VT, USA). In our laboratory, MicroTrace runs on PCs equipped with Windows (from 3.1 to Windows98). The program is used with Leica Medilux and Leica DMR light and fluorescence microscopes, equipped with stages and controllers from Märzhäuser GmbH (Wetzlar, Germany; scan 100 $\times$ 100 microscope stages, MCL or Multicontrol 2000 position control systems). Neurolucida was implemented on a PC running Windows 2000, coupled to a Zeiss Axiskop II light and fluorescence microscope, equipped with a scan 100 $\times$ 100 microscope stage and L-STEP position control system from Märzhäuser.

3.2. Automatic data acquisition: image analysis system

The software/hardware package employed was analySIS Pro v3.1 with the F-view camera for digital image acquisition (Soft Imaging System GmbH, Münster, Germany). The software runs on a Windows 2000 PC, and is used with Leica Medilux and Zeiss Axioskop II light and fluorescence microscopes, equipped with stages and controllers as described above.

3.3. 3D reconstruction

3D reconstruction of data recorded with the semi-automatic and automatic data acquisition systems was performed with the program Micro3D (Oslo Research Park, Oslo, Norway; see also http://www.nesys.uio.no). Micro3D was developed in our laboratory and used in several recent publications (see, e.g., Malmierca *et al* 1998, Vassbø *et al* 1999, Leergaard *et al* 2000a, 2000b, Leergaard and Bjaalie 2002, Bjaalie 2002). The digitized sections, acquired with both types of data acquisition, contained point and line coordinates (x, y) that were imported to Micro3D in ASCII format. Tissue shrinkage due to immunocytochemical processing was measured in the x, y-plane, and linear size adjustments were introduced to maintain correct *in vivo* proportions in the final 3D reconstructions. Micro3D was used to align the digitized sections interactively on the computer screen, using multiple anatomic landmarks and real time rotation of the reconstruction during alignment (explained in detail in, e.g., Leergaard *et al* 2000a, 2000b, Leergaard and Bjaalie 2002). Sections were assigned z-values defined by section thickness and serial numbers, before they were maneuvered into position. Surface rendering techniques available in Micro3D (for reviews, see Bjaalie *et al* 1997, Leergaard and Bjaalie 2002) were used to visualize contours as solid or transparent surfaces. The distribution of labelled structures was studied as dot maps and by density gradient analysis. Density maps were produced by dividing the image of the reconstruction, viewed from a particular angle, into squares of 5×5 μm using a grid, and assigning a colour code corresponding to the density of point coordinates within a radius of 100 μm centred on the square. To facilitate comparison of data, a local coordinate system for the pontine nuclei was applied (Leergaard *et al* 2000a, 2000b, Brevik *et al* 2001).

3.4. Assembly of illustrations

Photomicrographs were obtained through the F-view camera and analySIS software (Soft Imaging System GmbH Münster, Germany), and illustrations were assembled using Adobe Photoshop 6.0 and Adobe Illustrator 10.0. The grey-scale level and contrast level of the photomicrographs were optimized in Photoshop.

3.5. Software availability

Neurolucida and analySIS are commercially available software. MicroTrace is freeware available from the Neural Systems and Graphics Computing Laboratory, Oslo, Norway (http://www.nesys.uio.no). Micro3D is partly based on commercial graphics libraries, and is available for licensing through the Oslo Research Park, Oslo, Norway (see also http://www.nesys.uio.no).

4. Distribution of axonal plexuses labelled with light microscopic tracer

A series of 50 μm thick sections through the rat pontine nuclei was analysed. The sections contained axonal plexuses anterogradely labelled with BDA, following injection of this tracer

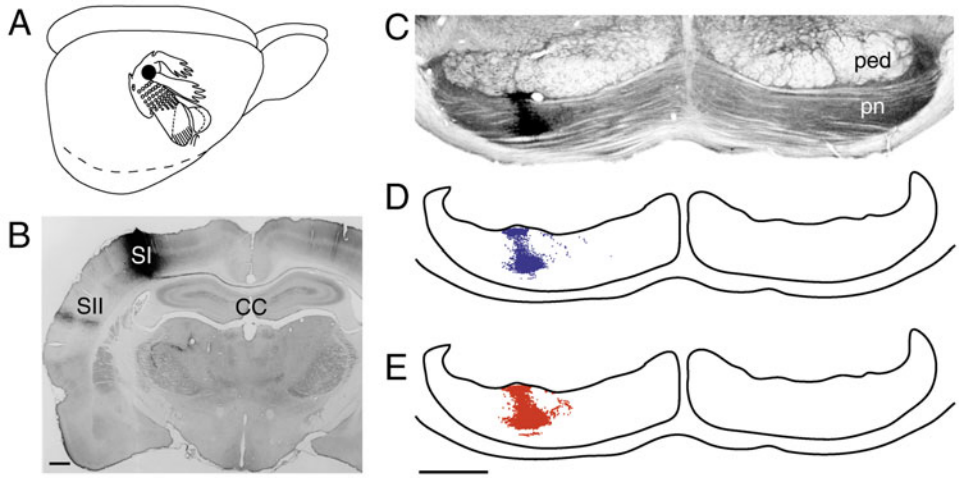

Figure 1. Axonal tracing in the rat cerebro-pontine system. The axonal tracer BDA was injected into the primary somatosensory region of the right cerebral hemisphere; position is indicated by a black dot in (A) (redrawn from Welker (1971) with permission). (B) shows a photomicrograph of a frontal section through the injection site. Labelling is visible in the secondary somatosensory cortex, the thalamus and in the corpus callosum. (C) shows a digital image (mosaic of 7×4 images) of a transverse section through the midpontine level in the same case. Two dense plexuses of BDA labelled fibres are visible close to the descending corticobulbar and corticospinal tract (peduncle). (D) and (E) show computerized plots of the same section as shown in (C), digitized using the semi-automatic method, computerized image-combining microscopy (D), and the automatic, image analysis method (E). CC, corpus callosum; SI, primary somatosensory cortex; SII, secondary somatosensory cortex; ped, peduncle; pn, pontine nuclei. Scale bars = 500 μm.

into the trunk representation of the primary somatosensory cortex (figure 1, experimental animal from Leergaard *et al* 2000b).

4.1. Semi-automatic digitization

With the computerized image-combining microscope (see technology section) anterogradely labelled axonal plexuses within the pontine nuclei were coded semi-quantitatively as points, using the 20× objective of the microscope. In areas with low density of labelling, point coordinates were placed at regular intervals along the length of single axons. In areas with dense labelling, a rough correspondence was sought between the density of labelling and the number of digitized points. The data were used for another purpose in Leergaard *et al* (2000b). Figure 1D shows a plot of the section shown in figure 1C.

4.2. Automatic digitization

The analySIS system (see technology section) was used for automatic data acquisition. The aim was to assign spatial coordinates to the tracer labelled axons in each section, comparable to the data obtained with the semi-automatic system. The steps involved were acquisition of a composite digital image from each section, definition of a threshold for the detection of labelling, and binarization.

The first step involved the use of the F-view camera, and the 10× objective of the microscope, for image acquisition. Exposure times were chosen to make grey tone

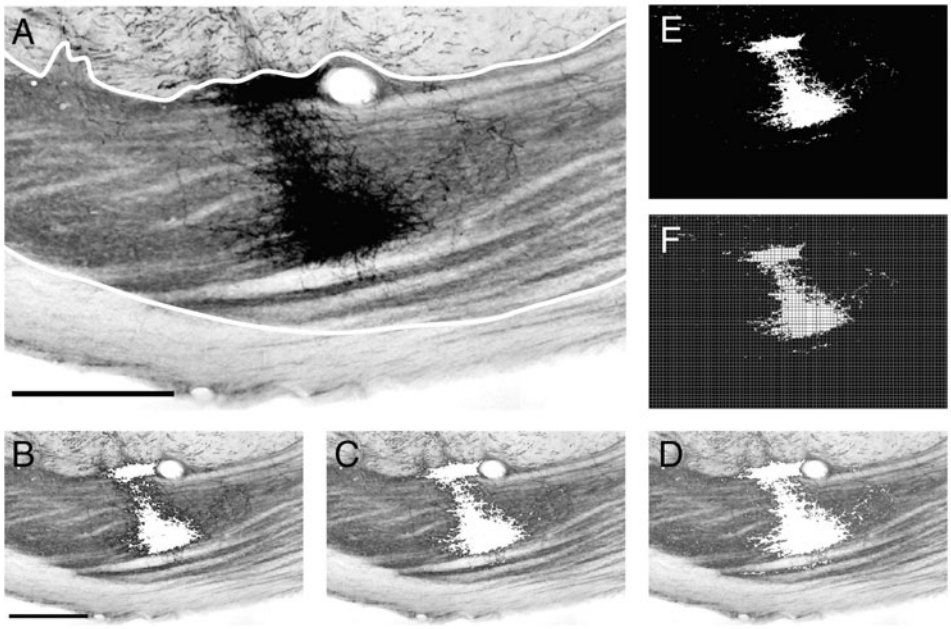

Figure 2. Automatic data acquisition of axonal labelling from a section through the pontine nuclei. (A) is a digital image of the same transverse pontine section as shown in figure 1(C), shown at a higher magnification. Crisp BDA labelled axons (black) are visible in dense and loose plexuses. The boundary of the pontine grey matter is indicated by a white line. Labelled fibres appeared as black or dark shades of grey and were identified from the digitized greyscale image by choosing a threshold value from minimum 0 (black) to a certain maximum level (dark grey). The images (B)–(D) show the results obtained with use of 'low', 'medium' and 'high' threshold levels, respectively. When the threshold was set too low, areas with low densities of labelled fibres were not identified (B). When the threshold was set too high, non-labelled structures were included (D). Thus, the accuracy of the data-acquisition depended critically on a significant signal to noise ratio between labelling and background, and a choice of threshold values that are neither too low nor too high (C). A binary image (E) was created based on the chosen threshold value (C). By superimposing a grid onto the binary image, it was possible to obtain x, y-coordinates from squares containing more than a given number of white pixels (F). Scale bars = 500 μm.

representation of labelled elements as uniform as possible. A mosaic of images, covering the region of interest, was recorded with use of the stepping motors of the microscope stage and the stage control functions and image alignment procedures in analySIS. The composite digital image in the section shown in figure 1C contained 7 $\times$ 4 images and covered an area of approximately 4200 μm $\times$ 1500 μm. Second, we analysed the part of the pontine nuclei containing most of the labelling (the right half, ipsilateral to the injection site, figure 2A). Differences in grey values were used to separate labelled fibres from background. Different ranges of grey values were tested. If the threshold value was set too low (figure 2B), areas containing weak labelling were not included. If the threshold value were set too high (figure 2D), non-labelled structures (darker parts in the digitized image) were included. We aimed at a threshold value that would avoid the inclusion of non-labelled structures, without losing much of the weak labelling. We could generally detect both the dense clusters of labelled fibres and some of the individual fibres adjacent to the clusters. (Weakly labelled regions could only be detected at the cost of including several non-labelled structures, see figure 2D.) Third, a binary image (figure 2E) was created on basis of the chosen threshold value (figure 2C).

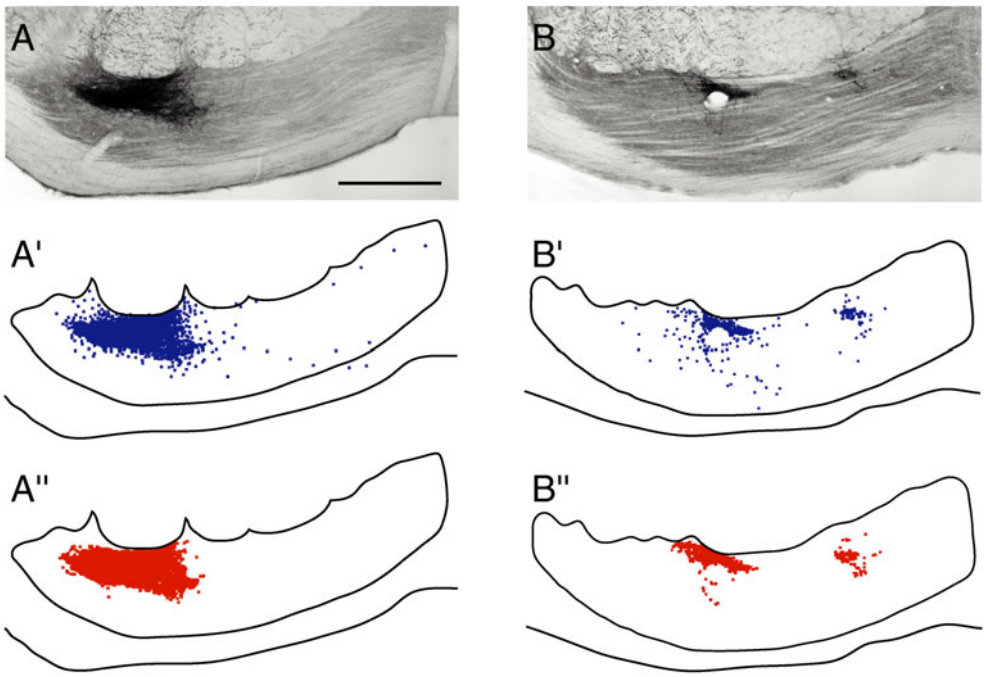

Figure 3. Comparison of plots of axonal distribution recorded with semi-automatic and automatic methods. (A) and (B) show digital images of transverse sections through the pontine nuclei, containing high (A) and low (B) densities of anterograde BDA labelling. (A′) and (B′) show computerized plots of BDA labelling acquired by the semi-automatic method (data from Leergaard *et al* (2000b)). (A″) and (B″) show plots of the same sections, obtained by the automatic method. Comparison of the two methods show that the distribution patterns are quite similar, but that the areas containing low densities of labelling are more emphasized in the semi-automatic plots (A′) and (B′). Scale bars = 500 μm.

A list of x, y-coordinates describing the location of the labelling (similar to the coordinates recorded with the semi-automatic system) was produced by

(1) superimposing a grid on the binary image,

(2) automatically identifying the squares in the grid containing more than a given number of white pixels, and

(3) recording the centre coordinate for each of these squares.

The step-wise procedure outlined above was performed section by section, to define x, y-coordinate lists of the distribution of labelling. The z-coordinates were derived from the serial number and thickness of each section. All steps were integrated in a macro, thereby significantly reducing the time spent for the data acquisition. The only manual procedure for each section was to adjust the range of grey values to best represent the distribution of the labelling. In addition to detecting the labelling, important anatomical landmarks were recorded and used as reference lines for 3D reconstruction (figure 2A, for more detailed considerations see Leergaard and Bjaalie 2002).

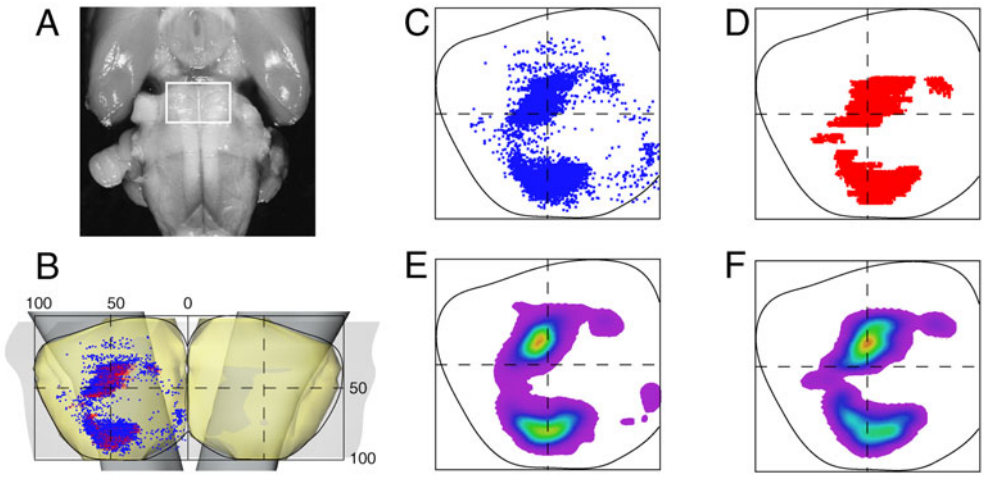

Figure 4. Computerized 3D reconstructions of a complete series of sections through the pontine nuclei (the same animal as shown in figures 1–3). (A) Image of a rat brain (ventral view). (B) 3D reconstruction of the pontine nuclei (ventral view). The ventral surface of the pons (grey) and the boundaries of the pontine nuclei (yellow) were shown as transparent surfaces and the reconstructed descending peduncles as solid surfaces dorsal to the pontine nuclei. A frame of reference is superimposed onto the reconstruction, and represents the local coordinate system for the pontine nuclei (explained in detail in Leergaard *et al* 2000a, 2000b, Brevik *et al* 2001). Relative coordinate values from 0 to 100% are used. The halfway reference lines are shown as dashed lines. BDA labelled corticopontine fibres distributed within the right pontine nuclei are represented as dots maps (C), (D) and as colour-coded density maps (E), (F), shown as total projections in views from ventral. The blue dots in (B) and (C) represent labelling recorded with semi-automatic data acquisition (data from Leergaard *et al* (2000b)), the red dots in (B) and (D) represent the same labelling recorded with the automatic method. The distribution patterns obtained with the two methods are quite similar. However, regions containing low densities of labelling are less emphasized in (D) and (F). Both density maps reveal similar rostrally and caudally located 'hot spots' of labelling (yellow to red colours in (E) and (F)).

4.3. Comparison and 3D analysis

Section by section analysis (figures 1 and 3) and 3D reconstruction (figure 4) were used for comparison of the results obtained with the semi-automatic and the automatic methods. Overall, the two methods produced comparable results. The automatic method was considerably less time-consuming than the semi-automatic method. High-density labelling, seen as densely packed clusters of labelled axons, was detected well with both methods. In the individual sections, the zones containing high densities of labelling were almost identically shaped, as recorded with the two methods (figures 1D, E, and 3A′, A″, B′ and B″). Density gradient analysis of the 3D reconstructions confirmed this impression (figure 4E, F). Low-density labelling, for example individual fibres outside the main clusters of labelling, or fragments of labelled fibres, was accurately recorded with the semi-automatic method. In the plots, such low-density labelling was seen as scattered dots (figure 3A′, B′, and 4C). The high precision could be confirmed by carefully comparing the plots with the images seen in the microscope. In comparison, many of the individual fibres and fibre fragments were not detected with the automatic method. In figure 3, the semi-automatic plots (A′ and B′) shows multiple data points corresponding to weak labelling that were not seen in the automatic plots (A″ and B″). The same difference was seen to advantage in the 3D reconstructions (compare

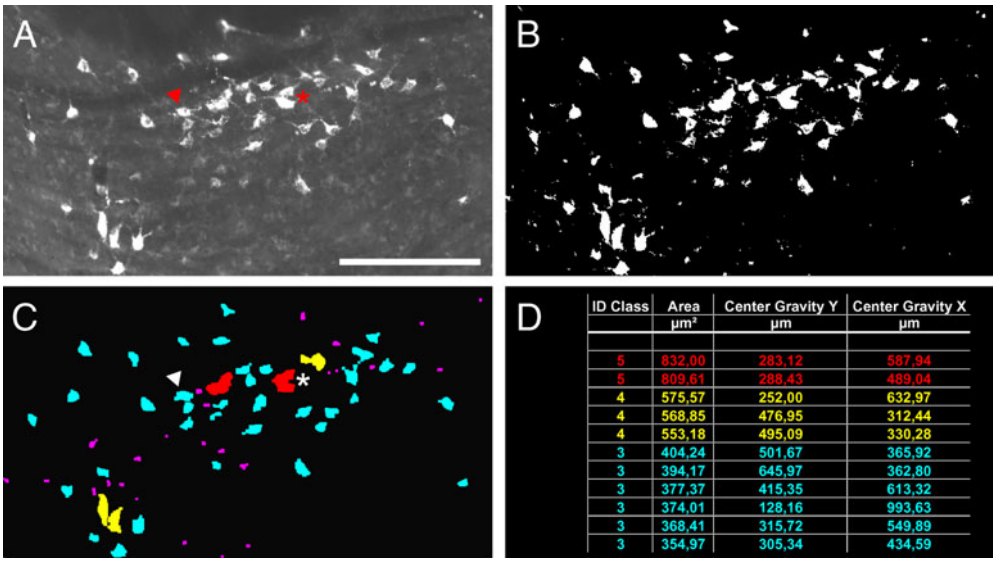

Figure 5. Detection of labelled cell distributions with an automatic method. (A) Digital greyscale image of transverse section through the pontine nuclei, showing pontocerebellar neurons labelled following injection of the fluorescent tracer rhodamine conjugated dextran amine (FluoroRuby, FR) into the cerebellar crus IIa. The digital image was converted to a binary black and white image by applying a threshold value (B). Binary operators were applied to remove artefacts, fill closed gaps and separate particles (see the text for a full description). Dense clusters of overlapping cells were not separated (asterisk), while partially overlapping cells, connected only by a thin bridge (arrow), were separated (C). A 'detect particle' function embedded in the analySIS software was used to count the resulting particles and sort them in a table according to area. A part of this table is shown in (D). Unique colours were assigned to different area ranges (C) and (D), and spatial coordinates (x, y) were automatically assigned to the centre of gravity of each particle (D). Careful comparison of the original 'raw image' with the analysed image shows that most labelled neurons are recognized correctly. Some cells, however, were not counted as separate objects due to the merging of overlapping cells. Weakly labelled cells, cellular fragments, and small artefacts (pink) that gave rise to particle sizes below the defined size (area) range for labelled cells were excluded from the output table. Scale bars $= 200\ \mu$m.

reconstruction from semi-automatically recorded data, shown in figure 4C, with reconstruction from automatically recorded data in figure 4D). In a few instances, weak labelling on a dark background could occasionally result in more data points with the automatic method (some of the small clusters of labelling in figure 1, compare the semi-automatically recorded plot in D with automatically recorded plot in E).

5. Distribution of neuronal cell bodies labelled with fluorescent tracer

A series of 50 μm thick sections through the rat pontine nuclei was analysed. These sections contained retrogradely labelled cells, following injection of FR into cerebellar cortex crus IIa. Figure 5A shows a representative microscope image of labelled cells. The labelled cell bodies appear bright, while unlabelled structures appear in darker shades. With the semi-automatic technique, the 20$\times$ objective was used and a point assigned to each cell body or larger fragment of a cell body. With the automatic technique, the 10$\times$ objective was used. Composite images were prepared following the same procedure as outlined for the fibre analysis above.

Again, exposure times were chosen to make grey tone representation of labelled elements as uniform as possible. The marked difference in brightness between the fluorescently labelled and unlabelled elements, and the limited variability in labelling intensity, made it possible to apply one threshold value for all sections. Based on the chosen threshold value, binary images were created (by applying the 'binarize' function available in analySIS, figure 5B) and particle identification in the software was employed. A particle in the binary image is a group of interconnected white pixels, surrounded by areas of black pixels. The aim was to represent each labelled cell body as a separate particle. To achieve this, we applied the erosion and dilation binary operators (see e.g., Mize *et al* 1988, Villa and Amthor 1995) and the 'separate particles' filter, available in analySIS. This made it possible to fill in gaps resulting from digitization of unevenly stained cells, to remove most of the artefacts (e.g., smaller objects, such as endothelial cells or other auto-fluorescent structures) and to separate several of the partly overlapping cells (figure 5C). The binary operators changed the shapes and outlines in the binary image. The area of each cell, however, was kept relatively constant by applying the same neighbourhood parameters to the erosion and dilation binary operators. Following these modifications of the images, we found it useful to divide the particles into different groups, based on the area of each particle (figures 5C, D). The aim was to give a size (area) range for labelled cells and to exclude particles with a size above or below this range. By measuring the average area of pontine neurons in a number of sections, we found a range that was likely to include cells and to exclude small artefacts due to autofluorescence. The end result was a coordinate list, with an x, y-coordinate and area assigned to each particle (figure 5D). Each particle was also given a unique number (not shown), which could be used to identify a specific particle in the original image. Such lists of x, y-coordinates from different sections, combined with the z-coordinates for each section, can be used as a basis for 3D-reconstruction, visualization and analysis of coordinate distributions, according to the principles described above.

We compared the semi-automatic and automatic plots of labelled cell distributions. In terms of number of labelled cells detected, the semi-automatic method typically recorded 10% more cells than the automatic method. By careful inspection, we found that the lower numbers recorded with the automatic method was mainly due to the merging of overlapping cell bodies (in places where the 'separate particle' filter did not succeed). Occasionally, weakly labelled cells were not detected with the automatic system. In a few places, non-neuronal structures with autofluorescence in the size range of the neurons were categorized as labelled cells with the automatic system.

6. Discussion

We have used two different data acquisition methods for recording the distribution of tracer labelled neuronal elements in tissue sections through the rat brain stem. The methods were computerized image-combining microscopy (a semi-automatic data acquisition method) and digital camera technology with image analysis software. We found that both methods were well suited for detecting dense clusters of labelled axons. The semi-automatic method was more suitable for detecting low densities of labelling, particularly individual axons and fragments or axons. Both methods were suitable for detection of the overall distribution of labelled cell bodies. In regions with a high density of labelled cells (overlapping cells), the automatic method was not capable of properly detecting individual cells.

Computerized image-combining microscopy has been used in hundreds of neuroscience investigations, not at least for studying the detailed organization of dendritic arbours (see, e.g. German *et al* 1985, Capowski 1985, Innocenti *et al* 1994, Cannon *et al* 1998, Reyes *et al* 1998, Stern and Armstrong 1998, Jacobs *et al* 2001). This semi-automatic method has long

been the method of choice for large-scale neuroanatomical analysis of neuronal organization at the individual cell level and at the level of neuronal populations. In our hands, and with the material and methods tested in this study, the image-combining method gave more accurate results than the automatic method. On the other hand, the image-combining method relied heavily on the ability of the user to identify all objects of interest, and slight differences in user interpretation could hardly be avoided. The method is also time-consuming when dealing with large numbers of objects to be digitized from multiple tissue sections.

Quantitative recording of dense axonal plexuses is a demanding task. Accurate tracing of individual axons and their arbours is feasible in experiments with small or intracellular tracer injections (Shinoda *et al* 2000, Kha *et al* 2001, Sugihara *et al* 2001). However, most systems anatomy investigations deal with densely labelled axonal plexuses, in which individual axons cannot be easily distinguished. Such plexuses may be characterized by delineating the boundaries of the labelled zones manually (Malmierca *et al* 1998) or by image analysis (Schwarz and Thier 1995, Schwarz and Möck 2001). Attempts to represent density variations within and around a labelled plexus include the semi-quantitative digitization employed in this study and by others (Leergaard *et al* 1995, 2000a, 2000b, Alloway *et al* 1998, 2000). The automated procedure for image analysis presented here represents a novel approach for characterizing labelled axonal plexuses more quantitatively.

Automatic data acquisition methods are hampered by several factors, such as possible lack of contrast between tracer and background (Schmitt and Eggers 1997), artefacts detected as labelled objects, weak labelling and uneven labelling. Nevertheless, the results obtained with the automatic approach tested in the present study clearly show that automatic approaches are suitable for detecting overall patterns of labelling through large brain regions. Hence, the continuously improving camera technologies and image analysis software now invite neuroanatomists to gradually modify their data acquisition strategy. The technology and software for automatic data acquisition tested in this study offered several advantages as compared to the image-combining method. First, it allowed extensive and convenient photo-documentation of all digitized sections. This is especially important when handling a material with fluorescent labelling that is susceptible to fading. Second, the automatic method was potentially more objective than manual plotting methods, since the only user controlled procedure introduced was the choice of threshold value.

Classical neuroanatomic investigations have usually relied on analysis of selected sections, such as one of five, or one of ten sections, through the brain region of interest. Local and global coordinate systems and 3D reconstruction are increasingly used to accurately define the spatial location of the tissue elements investigated (for review, see Bjaalie (2002)). There is increasing interest in new concepts for datasharing (Chicurel 2000, Koslow 2000, 2002, Bjaalie 2002), and in this context, more efficient strategies for handling of lower level data will be needed. The digital camera technology and databases integrated in the image analysis software offer convenient opportunities for establishing an internal laboratory database of image data, which in turn may serve as a basis for exporting such data to external, general neuroinformatics databases. With future refinement of software tools, for example, the use of more advanced methods for detecting and categorizing labelled objects in tissue sections, and the possible creation of new tools that combine properties of different data acquisition strategies, we expect that more automatic methods will gradually replace the time consuming manual methods. New automated methods for digitization of serial section data, combined with new tools for databasing and data sharing, may open new avenues for large-scale anatomical investigation of multiple brain systems.

Acknowledgments

We thank all contributors to the NeSys database (see references to individual articles)and Christian Pettersen for valuable technical assistance. Supported by The Research Council of Norway and EC grant QLRT-2000-02256.

References

Alloway K D, Mutic J J, Hoffer Z S and Hoover J E 2000 Overlapping corticostriatal projections from the rodent vibrissal representations in primary and secondary somatosensory cortex *J. Comp. Neurol.* **426** 51–67

Alloway K D, Mutic J J and Hoover J E 1998 Divergent corticostriatal projections from a single cortical column in the somatosensory cortex of rats *Brain. Res.* **785** 341–6

Amunts K and Zilles K 2001 Advances in cytoarchitectonic mapping of the human cerebral cortex *Neuroimag. Clin. N. Am.* **11** 151–69

Armstrong C L and Hawkes R 2000 Pattern formation in the cerebellar cortex *Biochem. Cell Biol.* **78** 551–62

Bjaalie J G 1992 Three-dimensional computer reconstructions in neuroanatomy. Basic principles and methods for quantitative analysis *Quantitative Methods in Neuroanatomy* ed M G Stewart (Chichester: Wiley) pp 249–93

Bjaalie J G 2002 Localization in the brain: new solutions emerging *Nat. Neurosci. Rev.* **3** 322–5

Bjaalie J G, Daehlen M and Stensby T V 1997 Surface modelling from biomedical data *Numerical Methods and Software Tools in Industrial Mathematics* ed M Daehlen and A Tveito (Boston, MA: Birkhauser) pp 9–26

Bjaalie J G, Diggle P J, Nikundiwe A, Karagülle T and Brodal P 1991 Spatial segregation between populations of ponto-cerebellar neurons: statistical analysis of multivariate spatial interactions *Anat. Rec.* **231** 510–23

Brevik A, Leergaard T B, Svanevik M and Bjaalie J G 2001 Three-dimensional computerized atlas of the rat brain stem precerebellar system: approaches for mapping, visualization, and comparison of spatial distribution data *Anat. Embryol.* **204** 319–32

Cannon R C, Turner D A, Pyapali G K and Wheal H V 1998 An on-line archive of reconstructed hippocampal neurons *J. Neurosci. Methods* **84** 49–54

Capowski J J 1985 The reconstruction, display, and analysis of neuronal structures using a computer microscope *The Microcomputer in Cell and Neurobiology Research* ed R R Mize (New York: Elsevier) pp 85–109

Capowski J J 1989 *Computer Techniques in Neuroanatomy* (New York: Plenum)

Chicurel M 2000 Databasing the brain *Nature* **406** 822–5

Danbolt N C, Chaudhry F A, Dehnes Y, Lehre K P, Levy L M, Ullensvang K and Storm-Mathisen J 1998 Properties and localization of glutamate transporters *Prog. Brain Res.* **116** 23–43

Flaherty A W and Graybiel A M 1994 Input–output organization of the sensorimotor striatum in the squirrel monkey *J. Neurosci.* **14** 599–610

German D C, Walker B S, McDermott K, Smith W K, Schlusselberg D S and Woodward D J 1985 Three-dimensional computer reconstruction of catecholaminergic neuronal popultions in man *Quantitative Neuroanatomy in Transmitter Research* ed L F Agnati and K Fuxe (London: Macmillan) pp 113–25

Glaser E M, Gissler M and Van der Loos H 1979 An interactive camera lucida computer-microscope *Soc. Neurosci. Abstr.* **5** 1697

Glaser E M, Tagamets M, McMullen N T and Van der Loos H 1983 The image-combining computer microscope—an interactive instrument for morphometry of the nervous system *J. Neurosci. Methods* **8** 17–32

Glaser J R and Glaser E M 1990 Neuron imaging with Neurolucida—a PC-based system for image combining microscopy *Comput. Med. Imag. Graph.* **14** 307–17

Glover J C, Petursdottir G and Jansen J K 1986 Fluorescent dextran-amines used as axonal tracers in the nervous system of the chicken embryo *J. Neurosci. Methods* **18** 243–54

Grefkes C, Geyer S, Schormann T, Roland P and Zilles K 2001 Human somatosensory area 2: observer-independent cytoarchitectonic mapping, interindividual variability, and population map *Neuroimage* **14** 617–31

He S Q, Dum R P and Strick P L 1993 Topographic organization of corticospinal projections from the frontal lobe: motor areas on the lateral surface of the hemisphere *J. Neurosci.* **13** 952–80

Heimer L and Zaborszky L 1989 *Neuroanatomical Tract-Tracing Methods 2. Recent Progress* (New York: Plenum)

Innocenti G M, Lehmann P and Houzel J C 1994 Computational structure of visual callosal axons *Eur. J. Neurosci.* **6** 918–35

Inoué S and Spring R 1997 *Video Microscopy: The Fundamentals* (Dordrecht: Kluwer)

Jacobs B, Schall M, Prather M, Kapler E, Driscoll L, Baca S, Jacobs J, Ford K, Wainwright M and Treml M 2001 Regional dendritic and spine variation in human cerebral cortex: a quantitative golgi study *Cereb. Cortex* **11** 558–71

Kha H T, Finkelstein D I, Tomas D, Drago J, Pow D V and Horne M K 2001 Projections from the substantia nigra pars reticulata to the motor thalamus of the rat: single axon reconstructions and immunohistochemical study *J. Comp. Neurol.* **440** 20–30

Köbbert C, Apps R, Bechmann I, Lanciego J L, Mey J and Thanos S 2000 Current concepts in neuroanatomical tracing *Prog. Neurobiol.* **62** 327–51

Koslow S H 2000 Should the neuroscience community make a paradigm shift to sharing primary data? *Nat. Neurosci.* **3** 863–5

Koslow S H 2002 Sharing primary data: a threat or asset to discovery? *Nat. Neurosci. Rev.* **3** 311–13

Lanciego J L and Wouterlood F G 1994 Dual anterograde axonal tracing with *Phaseolus vulgaris*-leucoagglutinin (PHA-L) and biotinylated dextran amine (BDA) *Neurosci. Protocols* 94-050-06-01-13

Leergaard T B and Bjaalie J G 1995 Semi-automatic data acquisition for quantitative neuroanatomy. MicroTrace—computer programme for recording of the spatial distribution of neuronal populations *Neurosci. Res.* **22** 231–43

Leergaard T B, Lakke E A and Bjaalie J G 1995 Topographical organization in the early postnatal corticopontineprojection: a carbocyanine dye and 3D computer reconstruction study in the rat *J. Comp. Neurol.* **361** 77–94

Leergaard T B, Alloway K D, Mutic J J and Bjaalie J G 2000a Three-dimensional topography of corticopontine projections from rat barrel cortex: correlations with corticostriatal organization *J. Neurosci.* **20** 8474–84

Leergaard T B, Lyngstad K A, Thompson J H, Taeymans S, Vos B P, De Schutter E, Bower J M and Bjaalie J G 2000b Rat somatosensory cerebropontocerebellar pathways: spatial relationships of the somatotopic map of the primary somatosensory cortex are preserved in a three-dimensional clustered pontine map *J. Comp. Neurol.* **422** 246–66

Leergaard T B and Bjaalie J G 2002 Architecture of sensory map transformations: axonal tracing in combination with 3-D reconstruction, geometric modeling, and quantitative analyses *Computational Neuroanatomy: Principles and Methods* ed G Ascoli (Totowa: Humana) at press

Malmierca M S, Rees A, Le Beau F E and Bjaalie J G 1995 Laminar organization of frequency-defined local axons within and between the inferior colliculi of the guinea pig *J. Comp. Neurol.* **357** 124–44

Malmierca M S, Leergaard T B, Bajo V M, Bjaalie J G and Merchan M A 1998 Anatomic evidence of a three-dimensional mosaic pattern of tonotopic organization in the ventral complex of the lateral lemniscus in cat *J. Neurosci.* **18** 10 603–18

Mize R R, Holdefer R N and Nabors L B 1988 Quantitative immunocytochemistry using an image analyzer: I. Hardware evaluation, image processing, and data analysis *J. Neurosci. Methods* **26** 1–23

Nadasdy Z and Zaborszky L 2001 Visualization of density relations in large-scale neural networks *Anat. Embryol.* **204** 303–17

Nikundiwe A M, Bjaalie J G and Brodal P 1994 Lamellar organization of pontocerebellar neuronal populations. A multi-tracer and 3D computer reconstruction study in the cat *Eur. J. Neurosci.* **6** 173–86

Rademacher J, Burgel U, Geyer S, Schormann T, Schleicher A, Freund H J and Zilles K 2001 Variability and asymmetry in the human precentral motor system. A cytoarchitectonic and myeloarchitectonic brain mapping study *Brain* **124** 2232–58

Reiner A, Veenman C L, Medina L, Jiao Y, Del Mar N and Honig M G 2000 Pathway tracing using biotinylated dextran amines *J. Neurosci. Methods* **103** 23–37

Reyes A, Lujan R, Rozov A, Burnashev N, Somogyi P and Sakmann B 1998 Target-cell-specific facilitation and depression in neocortical circuits *Nat. Neurosci.* **1** 279–85

Schleicher A and Zilles K 1990 A quantitative approach to cytoarchitectonics: analysis of structural inhomogeneities in nervous tissue using an image analyser *J. Microsc.* **157** 367–81

Schmitt O and Eggers R 1997 Systematic investigations of the contrast results of histochemical stainings of neurons and glial cells in the human brain by means of image analysis *Micron* **28** 197–215

Schwarz C and Thier P 1995 Modular organization of the pontine nuclei: dendritic fields of identified pontine projection neurons in the rat respect the borders of cortical afferent fields *J. Neurosci.* **15** 3475–89

Schwarz C and Möck M 2001 Spatial arrangement of cerebro-pontine terminals *J. Comp. Neurol.* **435** 418–32

Shinoda Y, Sugihara I, Wu H S and Sugiuchi Y 2000 The entire trajectory of single climbing and mossy fibers in the cerebellar nuclei and cortex *Prog. Brain. Res.* **124** 173–86

Stern J E and Armstrong W E 1998 Reorganization of the dendritic trees of oxytocin and vasopressin neurons of the rat supraoptic nucleus during lactation *J. Neurosci.* **18** 841–53

Sugihara I, Wu H S and Shinoda Y 2001 The entire trajectories of single olivocerebellar axons in the cerebellar cortex and their contribution to cerebellar compartmentalization *J. Neurosci.* **21** 7715–23

Swanson L W 2000 A history of neuroanatomical mapping *Brain Mapping. The Systems* ed A W Toga and J C Mazziotta (San Diego, CA: Academic) pp 77–109

Van Haeften T and Wouterlood F G 2000 Neuroanatomical tracing at high resolution *J. Neurosci. Methods* **103** 107–16

Vassbø K, Nicotra G, Wiberg M and Bjaalie J G 1999 Monkey somatosensory cerebrocerebellar pathways: uneven densities of corticopontine neurons in different body representations of areas 3b, 1, and 2 *J. Comp. Neurol.* **406** 109–28

Villa M F and Amthor F R 1995 Automating the quantitative analysis of 2D neural dendritic trees *J. Neurosci. Methods* **56** 77–88

Welker C 1971 Microelectrode delineation of fine grain somatotopic organization of (SmI) cerebral neocortex in albirno rat *Brain Res.* **26** 259–75

Wree A, Schleicher A and Zilles K 1982 Estimation of volume fractions in nervous tissue with an image analyzer *J. Neurosci. Methods* **6** 29–43

Zaborszky L and Duque A 2000 Local synaptic connections of basal forebrain neurons *Behav. Brain Res.* **115** 143–58